Biochar engineering and ageing influence the spatiotemporal dynamics of soil pH in the charosphere

Biochar engineering and ageing influence the spatiotemporal dynamics of soil pH in the charosphere

Xuejiao Chen [a,b*], Steven Lewis [c,d], Kate V. Heal [c,d], Qimei Lin [b], Saran P. Sohi [c,d]

[a] Institute of Urban Agriculture, Chinese Academy of Agricultural Sciences, Chengdu, 610213, China

[b] College of Land Science and Technology, China Agricultural University, Beijing, 100193, China

[c] School of GeoSciences, University of Edinburgh, Edinburgh, EH9 3FF, UK

[d] UK Biochar Research Centre, University of Edinburgh, Edinburgh, EH9 3FF, UK

[*] Corresponding author. Phone: +86 15652790103. E-mail address: chenxuejiao@caas.cn

Abstract

The charosphere, the interface microzone between biochar and soil, plays a vital role in biochemical processes following biochar application to soil. However, the development of the charosphere over time, and the pH dynamics within and around it, remain poorly understood as biochar ages. In this study, two kinds of biochars with distinct characteristics, a pristine biochar (BC_{SE}) and a hydroxyapatite engineered biochar (BC_{HA}), were subjected to artificial physicochemical ageing treatment. The localized impact of the fresh and aged biochars on soil pH were quantified, and spatiotemporal changes at the microscale visualized, using the planar optode technique. Association between the biochar characteristics and their charospheres were assessed using correlation and redundancy analyses to identify controls on charosphere properties.

Significant localized effects on soil pH were induced by biochar application, with pH gradients

around biochar particles forming gradually over 24 hours. Fresh biochars generated charospheres with radii ranging from 1.13 mm to 1.63 mm. However, ageing treatment slightly narrowed the charosphere radius to 1.08-1.12 mm. The spatiotemporal variations of pH in the charosphere were closely related to biochar characteristics. Ageing treatment resulted in large increases in the oxygen (91%-349%) and available phosphorus (670%-1094%) contents of biochar, but decreases in ash content (42%-45%), as well as pH (26%-54%) and electrical conductivity (EC) (17%-64%) values. The pore structure of biochar was altered and minerals were lost during the ageing process, so that aged biochars had much smaller specific surface area compared to the fresh biochars. Correlation and redundancy analyses revealed that the biochar EC value was the main factor determining the charosphere radius and pH within it. This study is the first to visualize and compare the charosphere derived from different fresh and aged biochars at a high resolution. The results provide new insight into the pH dynamics of the charosphere and the availability of elements as biochar ages following application to soil, which are important for understanding nutrient availability to plants and mobility of soil contaminants.

Keywords: biochar ageing, electrical conductivity, engineered biochar, pH gradient, temporal variation, planar optode

1. Introduction

Soil pH plays a critical role not only in nutrient cycling, but also in the translocation of potentially toxic elements (PTEs). For example, phosphorous (P) is most available for plants at pH 5.5-7.5. The solubility of P from alkaline Vertisols increased with acidification when soil pH was

below the threshold of approximately pH 6 (Andersson et al., 2015), while PTEs become soluble and potentially toxic to plant roots when soil pH falls below 5.5 (Neina, 2019). Biochar, well-known as a promising soil conditioner, has been reported to work well in increasing soil pH (Wu et al., 2020), thereby influencing the availability and mobility of both soil nutrients and contaminants (Melo et al., 2016; Kätterer et al., 2019). In addition, changes in soil pH induced by biochar application can affect the abundance and activity of soil micro-organisms, which further modulates various soil biochemical processes (Yu et al., 2019).

The effect of biochar on soil pH begins with small localized pH changes around the biochar particles once in the soil (Wang et al., 2017). Analogous to the rhizosphere, the soil volume adjacent to biochar particles and immediately affected by biochar is defined as the 'charosphere' (Lehmann et al., 2011; Quilliam et al. 2013), where the physicochemical properties differ significantly from those of the bulk soil (Luo et al., 2013). The charosphere has been shown to have pH 1.17-1.39 units higher than in unamended soil, locally decreasing the availability of cadmium (Cd) (Wang et al., 2017). Kuzyakov and Blagodatskaya (2015) considered the biochar-sphere (charosphere) could be a microbial hotspot, controlling biogeochemical processes and rates in the soil ecosystem. However, because of the microscale of the charosphere, traditional approaches, such as mesh separation (Houben and Sonnet, 2015), compartment rhizoboxes (Yu et al., 2019), and soil thin sections (Sauzet et al., 2017), cannot usually provide sufficient precision to probe biochemical processes within it. Moreover, research focusing on the dynamics of soil pH within the charosphere is sparse, so that our understanding is limited of the localized effects of biochars and their subsequent environmental influence.

Planar optodes (PO), a two-dimensional imaging system based on fluorescence measurement,

provide the capability to examine the spatial distribution of analytes with a high resolution (μm-mm) *in situ* and in real time (Santner et al., 2015; Li C. et al., 2019). Several studies have used PO to quantify the extent of the rhizosphere and investigate gradients of pH, O_2, and CO_2 that are closely related to physicochemical and biological processes in soil (Blossfeld et al., 2013; Faget et al., 2013; Koop-Jakobsen et al., 2018). In general, the extent of micro-zones measured by PO better represents their extent, approximately 3-5 times smaller, and gradients and processes within them, compared to traditional destructive methods (Kuzyakov and Razavi, 2019). In addition, when coupled with diffusive gradients in thin films (DGT), PO can further reveal the underlying mechanisms controlling the availability of soil P and PTEs, and microbial activities (Williams et al., 2014; Christel et al., 2016; Sun et al., 2019).

Liming is the primary factor leading to changes of soil pH. However, owing to a series of biotic and abiotic ageing processes, the liming effect of biochar could be short-lasting or even gradually decrease with time (de la Rosa et al., 2018; Duan et al., 2019). Ageing results in several changes in biochar, for example, decreased biochar pH and carbon (C) content (Li H. et al., 2019), but increases in hydrogen (H), oxygen (O) and O-containing functional groups (de la Rosa et al., 2018). Field experiments have revealed that ageing significantly altered the environmental behaviors of biochars and their interactions with soil nutrients and PTEs (Aller et al., 2017; Kumar et al., 2018; Gámiz et al., 2019; He et al., 2019). It can be inferred that the localized effects of biochar, especially on soil pH dynamics, will also be influenced by the changes in biochar properties due to ageing. In this study, the extent of the charosphere and the pH dynamics within it were investigated using the PO technique for two distinct biochars, with and without artificial ageing. The properties of the fresh and aged biochars were determined to help identify controls on the

charosphere characteristics. The research aims were to: 1) quantify the localized impact of biochar on soil pH, 2) visualize the spatial and temporal changes of soil pH following biochar addition, and 3) investigate how changes in biochar characteristics due to ageing determine the properties of the charosphere. The hypotheses were that: 1) the pH in the charosphere is distinct from that in adjacent bulk soil due to the significant localized effect of biochar, and 2) spatiotemporal pH changes in the charosphere are related to changes in biochar properties due to ageing. The results are expected to inform guidelines for effective utilization of biochar as a soil conditioner.

2. Materials and methods

2.1. Soil

Topsoil (0-20 cm, after removing surface vegetation) was collected from the Balruddery Research Farm (N 56°29′00.5, W 3°07′51.2″) of The James Hutton Institute, Dundee, Scotland, UK. The soil is a sandy loam developed on Old Red Sandstone geology of Devonian age and was collected from a riparian buffer strip with no recent history of fertilizer application to ensure low background soil P concentrations. On return to the laboratory, the soil was air-dried and crushed by hand with a pestle and mortar to pass through a 0.5 mm sieve. The soil characteristics are as follows: pH (H_2O, 1:2.5), 6.28; electrical conductivity (EC) (H_2O, 1:2.5), 1.16 mS cm^{-1}; sand 56.2%, clay 12.6%, silt 31.2%; organic matter content (loss on ignition), 7.34%; available P (Olsen extraction), 2.11 mg kg^{-1}; total P, 0.74 g kg^{-1}; total calcium (Ca), 2.38 g kg^{-1}; total nitrogen (N), 3.00 mg kg^{-1}; buffering capacity, 28.9 mmol (H^+) kg^{-1} soil pH^{-1}.

2.2. Biochars and ageing treatment

Oilseed rape (*Brassica napus* L.) (OR) is one of the most important oil crops worldwide with annual global production of 46 million t (FAOStat, 2018). As a result, numerous straw residues are generated each year, providing a good candidate raw material for biochar production. In this study, OR straw segments crushed to <2 mm were pretreated by steam explosion (SE) before pyrolysis at 500 °C for 2 h. The corresponding biochar (BC_{SE}) has a large surface area beneficial for retention of nutrients and adsorption of pollutants (Chen et al., 2019). The engineered biochar (BC_{HA}) was synthesized from SE-treated materials to create a new biochar with distinctive characteristics. Briefly, BC_{HA} was produced by immersing SE-treated OR straw in a hydroxyapatite (HAP) slurry created using 5-20 μm analytical grade HAP ($(Ca_{10}(PO_4)_6(OH)_2$, Sinopharm Chemical Reagent Co. Ltd., Shanghai, China) (Yang et al., 2016), and then pyrolyzing in the same conditions (500 °C, 2 h). More details of the biochar production and the characteristics of BC_{SE} and BC_{HA} are in Supplementary Material S1 and Table S1.

Generally, natural ageing of biochar occurs over several years to decades, or even longer (Cross and Sohi, 2013; Sun et al., 2020). To evaluate the long-term effect of biochar and accelerate the ageing process, BC_{SE} and BC_{HA} were artificially aged in the laboratory by physical and thermal chemical treatment using a method adapted from previous studies (Brabant, 2013; Cross and Sohi, 2013). Biochar (20 g) was weighed into a glass jar, followed by addition of 400 mL deionized water and 0.2 mL surfactant 2-octanol. After sealing the jar, the mixture was then shaken at 60 r min^{-1}, 25 °C for 1 h on an orbital platform shaker. The supernatant was discarded after standing for 10 min. This extraction was repeated another five times before oven-drying (80 °C) of the remaining biochar. Next, 5% hydrogen peroxide solution (H_2O_2) was added to the extracted biochar at a ratio of 70 mL

133 H_2O_2 to 1 g C of biochar. The new mixture was heated at 80 °C in an oven for 2 days with gentle
134 agitation 2 to 3 times per day, to ensure that all the biochar particles remained in suspension. The
135 oven temperature was increased to 105 °C on the third day to completely dry the biochar. The mass
136 loss of biochar, 1.97% and 1.72% for BC_{SE} and $BC_{HA,}$ respectively, was calculated by weighing the
137 biochars before and after the ageing treatment. The aged biochars were denoted as ABC_{SE} and
138 ABC_{HA}.
139
140 *2.3. Planar optode (PO) system and pH measurement*
141 The PO system consists of three parts: the sensing device, light source and signal capture
142 equipment, and information processing system (Faget et al., 2013; Li C. et al., 2019). The sensing
143 device is usually a permeable sensor foil only mm thick. Specific fluorophores in the foil move from
144 the ground state to the excited state once activated by light of a certain wavelength. The emitted
145 fluorescence signals during this process are closely related to the target analytes, e.g. H^+, O_2, CO_2,
146 in the matrix, and thus the concentration of a specific analyte can be determined after calibration of
147 the sensor foil under conditions of known analyte concentration. Relying on this optical technique,
148 the spatial and temporal changes of the analyte at sub mm scales can be accurately recorded by the
149 signal capture equipment and information processing system.
150 The PO system used in this study comprised a sensor foil (SF-HP5R, PreSens Precision
151 Sensing GmbH, Regensburg, Germany) with a measuring range of pH 5.5-7.5, a transparent vessel
152 to hold the samples and foils, and the VisiSens Detector Unit DU02 (PreSens GmbH) (Figure 1),
153 with excitation wavelengths pre-set by the manufacturer. The system allows pH quantification from
154 color ratiometric imaging, based on the fluorescence intensity ratio (*R* values) of the red and green

channels in the RGB images (1280 x 1024 pixels). The foils were calibrated with buffer solutions spanning a range of pH values using a 10-well CaliPlate (PreSens GmbH) (see Supplementary Material S2 for details) before pH imaging was conducted of the biochars in the study soil.

Foils from the same batch as the CaliPlate were cut into 1 cm × 1 cm squares and mounted using SG1 silicone glue (PreSens GmbH) in the center of plastic petri dish lids (diameter 89 mm). The foils were pressed down carefully to exclude air bubbles and the lids were placed in a dark room for at least 24 h for the glue to cure. The petri dish bases were then filled with soil that had been moistened with deionized water to 80% water holding capacity, and a biochar particle was placed in the center. The petri dishes were then closed and sealed, with the lid facing downwards so that the biochar particles and soil were in full contact with the sensor foils. All the prepared samples were measured one by one and installed in the same position as the CaliPlate (Figure 1).

Measurements were conducted in a dark room at a constant temperature (27±2 °C). The first image, i.e. the image at time 0 (T0), of each sample was taken at 5 min after biochar placement to allow time to set up the camera and measurement parameters in the system. Thereafter, the images were acquired automatically every 10 min for 24 h, with the last image recorded as T1. In total, 144 images (pixel size: ~32 μm) were acquired for each sample by the end of the measurement period. Three replicates of each biochar were measured.

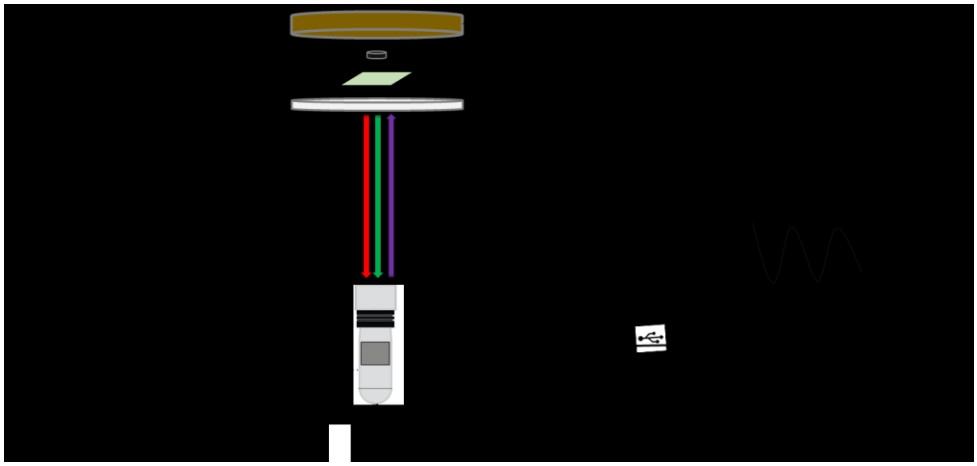

Figure 1. Schematic diagram of the set-up for pH mapping of the biochar in the study soil using the planar optode system.

2.4. Determination of biochar characteristics

The following characteristics were determined on three sub-samples of each of the four biochars used in this study. Biochar pH and EC were measured using calibrated probes and a multi parameter meter (HQ40D, HACH, USA) in deionized water at a ratio of 1:10 (w/v). Ash content and C, H, and N elemental contents were determined by loss on ignition in a muffle furnace (550 °C, 4 h) and an elemental analyzer (vario EL III, CHNOS Elemental Analyzer, Elementar Analysensysteme GmbH, Germany), respectively. Oxygen (O) content was calculated by percentage difference, i.e. O%=100-(C%+H%+N%)-ash%. Calcium (Ca) and phosphorous (P) were extracted by a modified dry-ash method for biochar. Specifically, 200 mg biochar was weighed into a crucible and heated in a muffle furnace (500 °C, 8 h). After cooling, the crucible was placed on a steam bath. Then, 5 mL of concentrated nitric acid (HNO_3) was added and evaporated to dryness. Next, 1 mL of HNO_3 and 4 mL of H_2O_2 were added and evaporated to dryness as well, followed by heating for a further 2 h. Once cool, the residues in the crucible were removed with 2 mL of HNO_3 and transferred with deionized water into a 50 mL volumetric flask through Whatman 4 filter paper.

The content of Ca and P in the filtrate was determined by inductively coupled plasma (ICP-OES, Thermo-iCAP 6300, Thermo Electron, USA). Available P was determined through water extraction (Prendergast-Miller et al., 2014) and measurement of the extracts using an autoanalyzer (Bran & Luebbe AA3, Seal Analytical, Norderstedt, Germany).

The surface morphology of the biochar samples (coated with a thin layer of gold) was examined using scanning electron microscopy (SEM) (S-3400N, Hitachi, Japan) (accelerating voltage: 3 kV, working distance: 7500-8200 μm). The functional groups of the biochars were characterized via Fourier transform infrared spectrometry (FTIR) (IS10, Thermofisher Nicolet, USA) (see Supplementary Material S3). The specific surface area (SSA) of a subsample from each biochar was determined (V-sorb 2008P Pore Analyzer, Gold APP, China) based on the multi-point Brunauer-Emmett-Teller (BET) adsorption isotherm. The volumes of meso/macropores and micropores in a subsample from each biochar were determined by the Barrett-Joyner-Halenda (BJH) and Saito-Foley (SF) methods, respectively.

2.5. Data processing and analysis

Image analysis was conducted in FIJI (Fiji Is Just ImageJ) software. The RGB images at the end of the 24 h measurement period were divided into red, green, and blue channels, from which the red to green composite images were generated for calculating the R values using the Image Calculator tool. The Plot Profile function was used to extract R values from a cross-section line along the central axis of the foil and bisecting the biochar particle. These were then converted to pH using the calibration equation (Supplementary Material S2) to obtain the spatial distribution of pH values. The temporal changes of pH within the regions of interest (ROIs) around the biochar

particles during the measurement period were obtained from all the images using the Z-axis Profile function in the VisiSens^{TM} AnalytiCal 2 software (PreSens, Germany). The mean *R* values of the pixels within each ROI were calculated and converted to pH in the software according to the calibration equation. This was conducted for all the biochar replicates and all images during the measurement period to generate pH mean and standard deviation values in all the ROIs for every 10 minute timestep.

The pH, EC, element composition, and ash content characteristics of the four study biochars were subjected to one-way analysis of variance (ANOVA), followed by least significance difference (LSD) tests in PASW Statistics18 software to identify significant differences. All data were shown to be normally distributed using the Shapiro-Wilk test. Correlation between the values of charosphere properties after 24 h and biochar characteristics was assessed using Pearson coefficients. In addition, redundancy analysis (RDA) was performed in Canoco 5.0 to identify the key biochar characteristics associated with the properties of the charosphere. The significance level in all statistical tests was $P<0.05$.

3. Results and Discussion

3.1. Spatial distribution of pH in charospheres around different biochars

At the end of the experiment, soil pH declined with distance from the biochar particles towards the initial value for the bulk soil (pH 6.28), most notably for the fresh biochars. The highest pH values were detected immediately adjacent to the biochar particles (Figure 2), indicating a significant localized effect of biochar on soil pH. In this study, the biochar influence on soil pH is defined as the diameter of influence (Φ), which was quantified as the distance from the center of the

234 biochar particle along which the pH is outside pH 6.07-6.49 (mean bulk soil pH 6.28±0.21, 1
235 standard deviation). Both BC_{SE} and BC_{HA} increased the soil pH to more than 6.49 and had diameters
236 of influence of 5.56 mm and 3.79 mm, respectively (Table 1). Yu et al. (2019) reported a similar
237 spatial pattern in soil pH with distance from biochar, which they attributed to the diffusion of
238 minerals, such as K, Ca, and Mg, from the biochar surface. In the present study, more mineral
239 diffusion is expected from BC_{SE} due to its higher EC value (4.37 mS cm^{-1}), compared to BC_{HA} (2.72
240 mS cm^{-1}) (Table S1). This might explain the larger diameter of influence on soil pH of BC_{SE} than
241 BC_{HA}. In comparable experiments with particles of other biochars placed in pH 4.9 soil, Buss et al.
242 (2018) showed that the soil pH increased over a greater distance (~5.2 mm) for the biochar with
243 greater EC value and particle size. The mean diameter of BC_{SE} and BC_{HA} particles in this experiment
244 was 2.30 mm and 1.54 mm, respectively (Table 1). However, the ratio of the charosphere radius to
245 biochar radius was very similar for both the fresh biochars (BC_{SE} 1.42, BC_{HA} 1.47), suggesting there
246 is no significant difference in soil pH influence per mm diameter of these biochar particles.
247 Ageing treatment led to notable changes in the soil pH spatial distribution and gradient of
248 change around the biochar particles. The pH gradient surrounding the aged biochar ABC_{SE} was not
249 as steep as that of the fresh biochars (BC_{SE} and BC_{HA}) (Figure 2). The diameter of influence (Φ) of
250 ABC_{SE} on soil pH (4.33 mm) was smaller than that induced by BC_{SE} (5.56 mm) (Table 1). The
251 acidic nature of ABC_{HA} resulted in a localized decrease in pH below 6.07 with a diameter of 4.39
252 mm (Figure 2; Table 1). Furthermore, the ratios of the charosphere radius to biochar radius were
253 1.07 and 0.97 for ABC_{SE} and ABC_{HA}, respectively, significantly lower than that for BC_{SE} and BC_{HA}.
254 Thus, it is apparent that ageing reduced the localized influence of biochar on soil pH. In this study,
255 fresh biochars generated charospheres with radii (r) ranging from 1.13 mm to 1.63 mm. However,

the aged biochars had slightly narrower charospheres, 1.12 mm and 1.08 mm for ABC_{SE} and ABC_{HA}, respectively (Table 1). Yu et al. (2019) detected significantly higher soil pH in the near charosphere zone (~1 mm), compared to the far charosphere zone (2-5 mm) and bulk soil (> 5 mm). Within the charosphere of BC_{SE}, BC_{HA} and ABC_{SE}, soil pH was higher than that in bulk soil (Figure 2), which indicates their potential benefit for immobilizing PTEs, such as Cd^{2+}, Pb^{2+}, and Zn^{2+}, although this benefit might decrease as the biochars age.

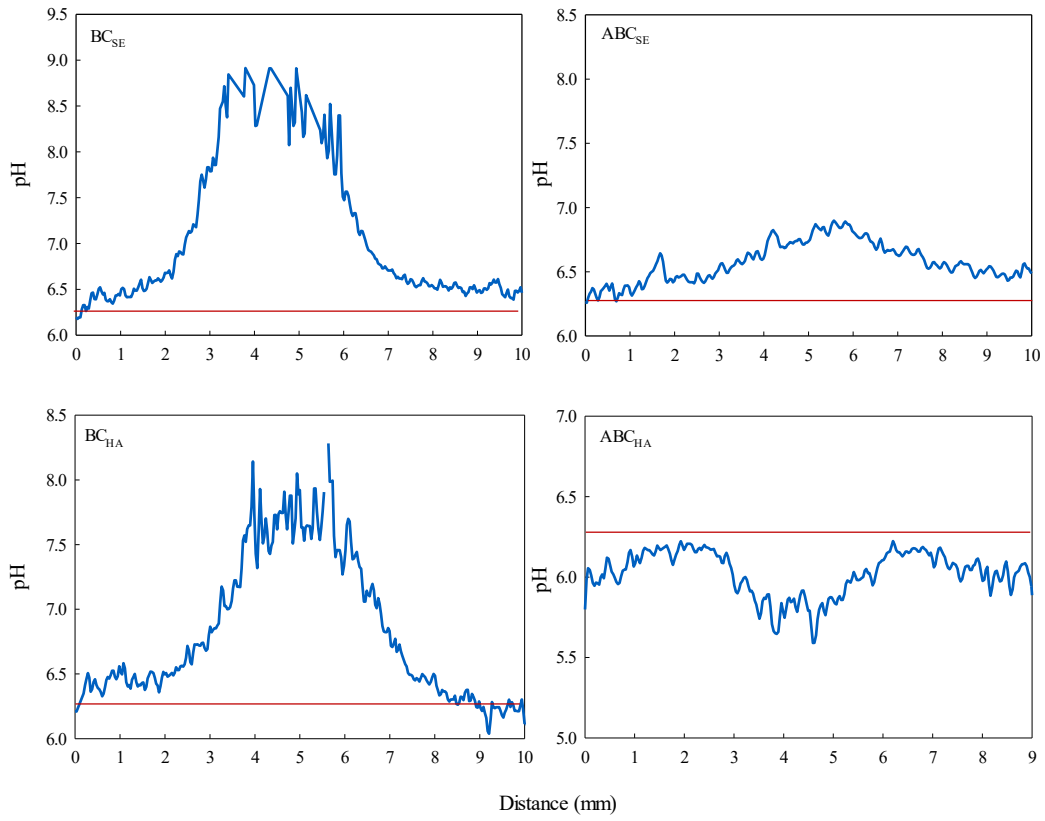

Figure 2. pH spatial variation along the cross-section of moist soil amended with different biochars 24 h after biochar addition. Note different y-axis scales.

(The vertical grey shaded areas show the position of the biochar particle. The red solid lines and surrounding horizontal pink shaded areas represent the mean bulk soil pH 6.28±0.21, 1 standard deviation. The pH gradients were similar around the three replicates analyzed of each biochar, so data for only one replicate are shown here).

Table 1. Particle size of the biochars used in the experiments and their diameter of influence and charosphere radius based on soil pH change 24 h after biochar addition to soil

Biochar type	Biochar particle size (mm)	Diameter of influence (Φ) (mm)	Charosphere radius (r) (mm)
BC_{SE}	2.30±0.88	5.56±0.98	1.63±0.32
ABC_{SE}	2.10±0.36	4.33±0.54	1.12±0.18
BC_{HA}	1.54±0.55	3.79±0.29	1.13±0.14
ABC_{HA}	2.23±0.25	4.39±0.70	1.08±0.23

The biochar particle size and diameter of influence are the maximum diameters as quantified by the function *Feret's diameter* in ImageJ. The charosphere radius was calculated as the difference between the radius of the biochar particle and its influence on soil pH as explained in section 3.1. All values are means ± 1 standard deviation (SD), n=3.

3.2. Temporal variation of pH in the charosphere

To better understand the pH dynamics, the soil covered by the sensor foil was divided into three regions of interest (ROIs): the biochar particle (#1), the immediate vicinity of the biochar (#2), and the bulk soil (#3) (Figure 3). During the 24 h experiment, the influence of the biochars on soil pH expanded continuously (Appendix B), apart from in the outermost region #3 within the first 2 h after biochar addition, when the soil pH value fluctuated slightly by 0.1-0.2 units. A possible reason for this variability is that pH oscillated across the whole experimental system at the start of the experiment due to soil disturbance (mixing and wetting), but in regions #1 and #2 this pH response was overwhelmed by the effect of the biochar on soil pH. Over time, soil pH initially increased in regions #1 and #2 around BC_{SE}, BC_{HA} and ABC_{SE}, but decreased in the same regions around ABC_{HA}, before reaching equilibrium. Irrespective of biochar type, the time to equilibrium pH in region #1 was always shorter than in #2 (Figure 3), indicating a gradual release and diffusion of compounds from the biochar. Generally, the time for formation of pH gradients within the charosphere varies from a few hours to days, driven by rapid dynamic processes, such as sorption and diffusion (Buss

et al., 2018; Koop-Jakobsen et al., 2018). However, the establishment of specific microbial communities in response to these gradients occurs over longer timescales (Kuzyakov and Razavi, 2019).

In region #1 (the biochar particle), the maximum pH values for BC_{SE} and BC_{HA} were no more than 7.5 and for ABC_{HA} the minimum pH values were approximately 5.4 (Figure 3) because the accurate measurement range of the SF-HP5R foil is pH 5.5-7.5. At the end of the experiment after 24 h, the soil pH at the interface between biochar and soil was distinct from those of the biochar particle and the bulk soil. For the BC_{SE}, BC_{HA} and ABC_{SE} biochars, the pH values in the different regions were in the order #1 > #2 > #3, whilst the opposite order occurred around the ABC_{HA} biochar, due to its acidic nature. The differences in pH value between regions #2 and #3 of BC_{SE} and BC_{HA} were 0.62 and 0.74 units, respectively, whereas that of ABC_{SE} and ABC_{HA} were only 0.13 and 0.27 units. It is thus apparent that the fresh biochars had a stronger effect on soil pH compared to the aged biochars. Although the soil pH values in region #3 were pH 6.03-6.28 at 24 h after biochar addition, similar to the bulk soil pH (6.28 ± 0.21), the PO technique allows continuous monitoring of pH *in situ* and at a fine resolution to identify the development of the charosphere and its distinct characteristics which is not possible with destructive measurement techniques applied to bulk soil samples.

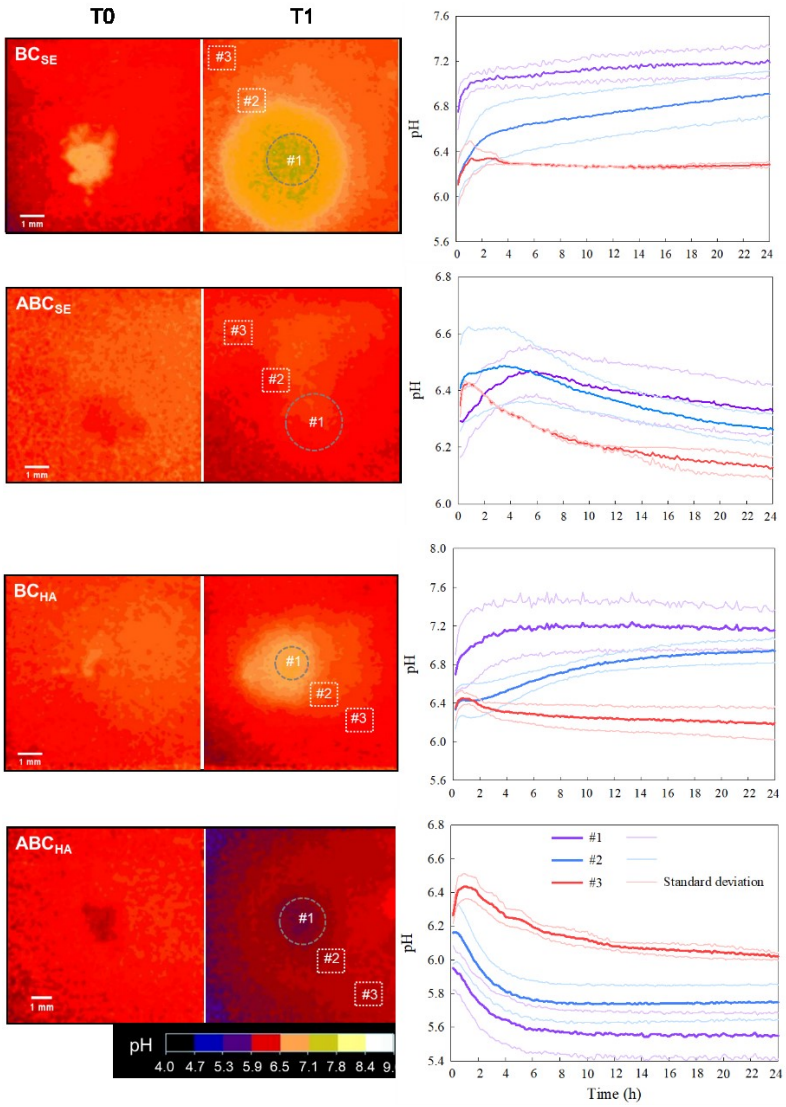

Figure 3. Temporal variation of soil pH after amendment with different biochars.

(The left hand panels show images of the 2D pH values of one of the replicates for each biochar at the start (T0) and end (T1) time of measurement, respectively. Pixel size: 1 pixel ~32 µm. In the T1 images the grey circle #1 indicates the position of biochar particles and the white rectangles #2 (immediate vicinity of the biochar) and #3 (bulk soil) refer to the ROIs for pH analysis. The right hand panels show pH means ± 1 SD (the pale color lines), calculated every 10 minutes for the 3 replicates for the corresponding ROIs. Note different y-axis scales).

3.3. Effects of ageing treatment on biochar properties

3.3.1. pH and EC

Both BC_{SE} and BC_{HA} biochars were strongly alkaline with pH values of 9.27 and 9.58, respectively (Table S1). The pH of the engineered biochar (BC_{HA}) was higher owing to HAP which

contains alkaline substances, such as carbonates and calcium hydroxides (Figure S2) (Pereira et al., 2015; Yang et al., 2016). The ageing treatment greatly reduced the pH of the aged ABC_{SE} and ABC_{HA} biochars to pH 6.87 and 4.39, respectively, which were 26% and 54% lower than that of their fresh biochars (Figure 4). One reason for these pH decreases might be the increase in acidic functional groups, such as carboxyl (Figure S2), on the biochar surface resulting from the intense oxidation action of H_2O_2 (Kumar et al., 2018). Another contributing factor is the loss of ash and alkaline components in the repeated extractions during the ageing process since the ash contents of ABC_{SE} and ABC_{HA} were only half that of BC_{SE} and BC_{HA} (Table 2). The EC values of biochars also decreased by 17-64% after ageing treatment (Figure 4). In particular, the EC value of BC_{SE} fell sharply from 4.37 mS cm^{-1} to 1.59 mS cm^{-1}, indicating that a large amount of soluble salts had disassociated from the biochar during the ageing treatment. Spokas et al. (2014) also observed that various inorganic salts (e.g. K, Cl, Ca, P) coating the biochar surface were dissolved and disappeared after rinsing with water for 24 h.

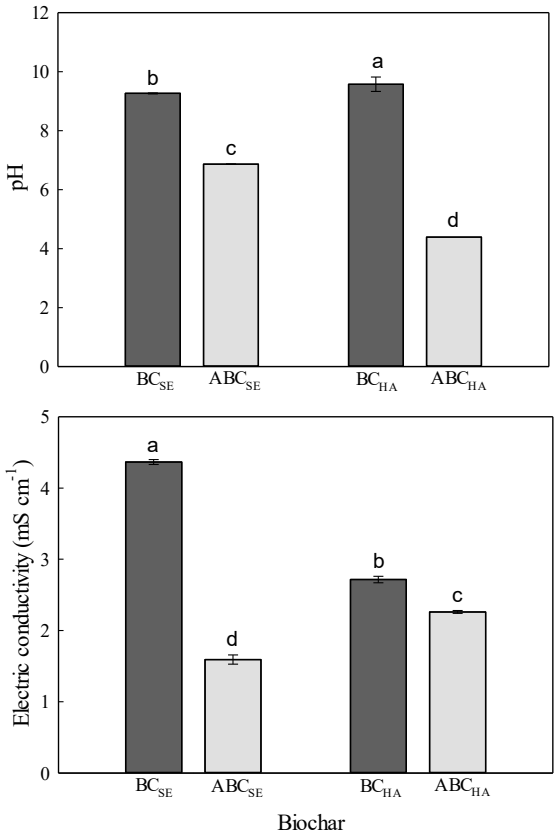

Figure 4. pH and EC values of the fresh pristine (BC_{SE}) and engineered (BC_{HA}) biochars and their aged biochars (ABC_{SE}, ABC_{HA}).

(All values are means ± 1 SD, n=3. Different lowercase letters above the bars indicate significant differences, $P<0.05$).

3.3.2. Element composition and ash content

The pristine biochar BC_{SE} contained more C (66.6%), H (2.66%), and N (1.20%) compared to the engineered biochar BC_{HA} (Table 2). Hydroxyapatite modification introduced more minerals, so BC_{HA} had a 132% higher ash content, but 54% lower O content than BC_{SE}. Ageing treatment did not significantly affect the C content, but increased the O content in ABC_{SE} and ABC_{HA} to 23% and 25%, respectively, which were 2 and 4 times the amount in their corresponding fresh biochars. The increase in O is attributed to both the loss of ash following repeated extractions and the extremely strong oxidation by H_2O_2 during the ageing treatment. Previous studies have consistently reported that surface oxidation is one of the major reactions during biochar ageing (Cheng et al., 2008; Huff

and Lee, 2016; Kumar et al., 2018), which is also confirmed by the shift and wider absorption peak of –OH in the FTIR spectra (Figure S2). The newly formed O-containing functional groups are helpful in increasing the cation exchange capacity of biochar (Rechberger et al., 2019) and thus its adsorption capacity for cations. Furthermore, the higher O/C ratios of ABC_{SE} and ABC_{HA} compared to their fresh biochars indicate the enhancement of polarity but reduction of stability (Spokas, 2010; Schimmelpfennig and Glaser, 2012; de la Rosa et al., 2018).

The Ca (48 g kg^{-1}) and total P (21 g kg^{-1}) contents in BC_{HA} were significantly higher than that of BC_{SE} (Table 2), because HAP is a naturally mineralized calcium apatite, as revealed by the absorption peaks at 963 cm^{-1} and 628 cm^{-1} in the FTIR spectra (Figure S2), corresponding to the bending vibration of the P-O bond and the stretching vibration of PO_4^{3-}, respectively (Yang et al, 2016). Ageing treatment resulted in decreases of approximately 50% in biochar ash content. Moreover, the total Ca and P content of ABC_{HA} were 38% and 42%, respectively, lower than that of BC_{HA}, suggesting that components containing them had disassociated during ageing. It is reported that the loss of alkali metal salts is the primary reason contributing to the decrease of biochar pH during ageing (Kumar et al., 2018; Tan et al., 2020). Surprisingly, the biochar water extractable P contents increased dramatically after ageing treatment in this study, by an order of magnitude in ABC_{SE} and ABC_{HA} compared to their fresh biochars (Table 2). Physical breakdown of the biochar structure induced by repeated shaking during the water extraction is one possible explanation for this observation. By promoting fresh exposure of biochar surfaces and fissuring (Spokas et al., 2014), ageing treatment might accelerate hydrothermal reactions and decomposition of the inert P fraction in biochar. Therefore, it can be speculated that the availability of minerals, such as P, may be enhanced during biochar ageing, which is beneficial for supporting plant nutrition.

369 Table 2. Element composition and ash content in fresh (BC_{SE}, BC_{HA}) and aged (ABC_{SE}, ABC_{HA}) biochars

Biochar	C	H	O	N	Atom H/C	Atom O/C	Ca	P	Water extractable P	Ash
	(%)						($g\ kg^{-1}$)		($mg\ kg^{-1}$)	(%)
BC_{SE}	66.6±0.13 a	2.66±0.06 a	12.0±0.12 b	1.20±0.04 a	0.48±0.01 b	0.14±0.00 c	11.2±1.59 c	1.22±0.18 c	41.3±8.50 c	17.5±0.17 c
BC_{HA}	51.0±0.10 b	2.25±0.05 c	5.47±0.43 c	0.62±0.02 d	0.53±0.01 a	0.08±0.01 c	47.9±3.81 a	21.2±1.60 a	435±36.6 b	40.7±0.48 a
ABC_{SE}	64.0±1.84 a	2.45±0.06 b	23.0±1.82 a	0.89±0.03 b	0.46±0.01 b	0.27±0.03 b	9.66±0.46 c	1.14±0.07 c	318±15.9 b	9.66±0.04 d
ABC_{HA}	49.0±2.37 b	2.20±0.07 c	24.6±2.28 a	0.78±0.06 c	0.54±0.03 a	0.38±0.05 a	29.5±0.77 b	12.2±0.29 b	5191±399 a	23.5±0.03 b

370 All values are means ± 1 SD, n=3. Different lowercase letters in the same column indicate significant differences (P<0.05).

371 *3.3.3. Surface morphology and pore structure*

372 Biochar derived from slow pyrolysis at 500 °C (BC_{SE} and BC_{HA}) largely retained the original
373 vascular structure of oilseed rape straw. Debris and mineral granules in the feedstock were entrained
374 inside the pores of fresh biochar (Figure 5). Ageing treatment seemed to 'clean up' the biochar,
375 resulting in a smoother surface and clearer pore structure, aligned with similar results from Jing et
376 al. (2018). In addition, there was a sharp decrease in the surface area of biochar from 73.7 $m^2\ g^{-1}$
377 (BC_{SE}) and 226 $m^2\ g^{-1}$ (BC_{HA}) to 2.23 $m^2\ g^{-1}$ (ABC_{SE}) and 1.73 $m^2\ g^{-1}$ (ABC_{HA}), respectively, after
378 the ageing treatment. The total pore volume of biochar reduced by 86-95% as well. The mean pore
379 size of ABC_{SE} and ABC_{HA} were 14.6 nm and 15.8 nm, respectively, which was 4 to 5 times the size
380 in their fresh biochars (Table 3). Consequently, in this study, exposure to leaching by water and
381 H_2O_2 during the ageing treatment reduced the number of pores in the biochars, whilst at the same
382 time enlarging the size of the remaining pores.

383 Nevertheless, how ageing affects biochar surface area and pore structure is not clear cut, as
384 results vary between studies. For instance, Feng et al. (2018) reported from laboratory experiments
385 that biochar pores were damaged when constantly exposed to air or flushed by neutral and acidic
386 solutions, and the surface area of biochar was reduced by ~40%. Yi et al. (2020) noted smoothing
387 of the internal biochar surface 2 years after burial in the field, but subsequent physical fragmentation
388 and collapse of large pores and an increase in micropores with the prolongation of ageing time.
389 Overall, the effect of ageing on biochar morphology and pore structure, depends not only on the
390 duration of ageing and the environmental conditions, but also on the biochar composition and
391 surface characteristics (Spokas et al., 2014; Rechberger et al., 2017; Liu et al. 2019). The greater
392 decrease in the surface area of BC_{HA} compared to BC_{SE} after ageing in this study is attributed to the

dissociation of HAP that has numerous micropores and a high surface area (Pastore et al., 2020). During ageing treatment, HAP that was loosely bound onto biochar was readily detached, resulting in the decreased total Ca and P content of ABC_{HA} (Table 2), as well as a reduction in surface area.

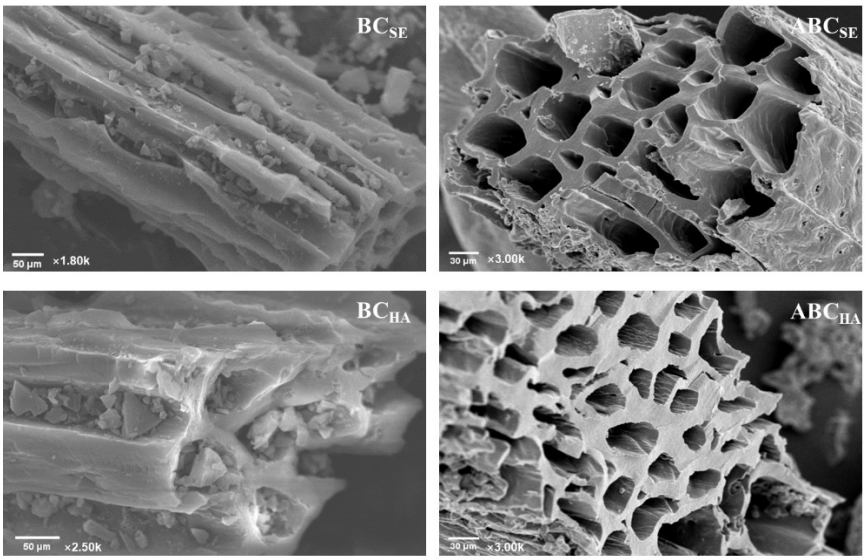

Figure 5. Representative SEM images of the fresh (BC_{SE}, BC_{HA}) and aged (ABC_{SE}, ABC_{HA}) biochars.

Table 3. The surface area and pore structure of different fresh (BC_{SE}, BC_{HA}) and aged (ABC_{SE}, ABC_{HA}) biochars

Biochar type	SSA ($m^2\ g^{-1}$)	V_{total} ($cm^3\ g^{-1}$)	V_{micro} ($cm^3\ g^{-1}$)	$V_{meso/macro}$ ($cm^3\ g^{-1}$)	MPS (nm)
BC_{SE}	73.72	0.07	0.03	0.05	4.03
BC_{HA}	225.68	0.19	0.09	0.12	3.35
ABC_{SE}	2.23	0.01	0.08×10^{-2}	0.82×10^{-2}	14.6
ABC_{HA}	1.73	0.01	0.07×10^{-2}	0.67×10^{-2}	15.8

SSA: Specific surface area; V_{total}: Total pore volume; V_{micro}: Micropore volume; $V_{meso/macro}$: Meso/macropore volume; MPS: Mean pore size (diameter).

3.4. Biochar characteristics related to the properties of the charosphere

The function of biochar in soil is greatly dependent on the biochar characteristics (Naisse et al., 2013; Kambo and Dutta, 2015), therefore the properties of the charosphere are expected to be closely related to those of the biochars themselves. In this study, redundancy analysis (RDA) showed that biochar characteristics overall explain 88.6% of the variability in the response variables (Table S2), i.e. the charosphere pH, diameter of influence (Φ) and charosphere radius (r) 24 h after biochar application. Among the explanatory variables for the charosphere properties, biochar EC contributed the most (40.5%), followed by particle size (PS) and biochar pH at 33.9% and 15.1%, respectively. The biochar EC values were closely positively related to the charosphere radius (r) (Figure 6), suggesting a significant role of dissolved salts following biochar application. The development of the charosphere radius observed during the 24 h time period of this study (Appendix B) appears to be strongly related to the dissolution of soluble minerals from biochar over time. Ageing treatment led to dramatic decreases in biochar EC values (Figure 4), which could be why the fresh biochars affected the soil pH over a wider area than the aged biochars (Table 1). Thus, it is speculated that the localized effect of biochar on soil pH will gradually slow down over time following application to the soil. Both the results from the present study and Buss et al. (2018) demonstrated that the particle size is another factor determining the extent of the localized effect of biochar, while the charosphere pH ($pH_{charosphere}$) is positively correlated to that of biochar ($pH_{biochar}$) (Figure 6).

Correlation analysis further confirmed the close associations between biochar and charosphere properties (Table 4). The Pearson coefficients between biochar EC and charosphere pH, diameter of influence (Φ), as well as the charosphere radius (r) were all significantly positive. In addition, the

very high positive Pearson coefficient between $pH_{biochar}$ and $pH_{charosphere}$ (0.970, $P<0.01$) indicates that biochar pH directly affects the charosphere pH, and thus is an important driver of the environmental effects of biochar application. Interestingly, the biochar water extractable P content (WP) was significantly positively associated with H/C and O/C ratios, yet negatively correlated with both $pH_{biochar}$ and $pH_{charosphere}$ ($P<0.01$), indicating important interactions between biochar properties, biochar ageing, and pH and phosphorus dynamics in the charosphere. The higher WP of the ABC_{SE} biochar demonstrated that hydroxyapatite modification of biochar can enhance its suitability as a P fertilizer, even though the charosphere radius of this biochar (1.12 mm) was smaller than that of the pristine BC_{SE} (1.63 mm). The final pH values in the charosphere 24 h after biochar application were 5.7-6.9 (Figure 3, ROI #2), which is within the suitable range of soil pH for a high P availability. The pH of the charosphere around the aged biochars was much lower than that of the fresh biochars. In particular, the $pH_{charosphere}$ following ABC_{HA} application was less than 5.8, well below the pH value of the bulk soil (6.28). Pastore et al. (2020) pointed out that acidification is the main mechanism of P solubilization from hydroxyapatite, and moreover, acidic functional groups can dissociate protons and promote the release of phosphate. Therefore, the decreased pH as well as enrichment in acidic functional groups observed after the ageing treatment are further possible reasons for the large increase in water extractable P in the aged biochars (Table 2). Whilst the biochar ageing process appears to be helpful for P release and providing available P to plants, the concurrent decreased liming effect might increase the risk of desorption of PTEs originally adsorbed onto biochar.

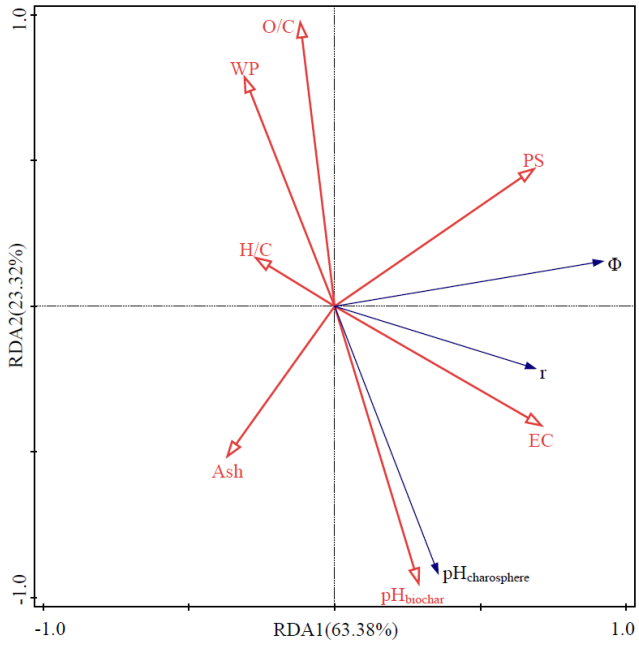

Figure 6. Ordination biplot of redundancy analysis (RDA) axis 2 against RDA axis 1 conducted on the response variables (charosphere properties) and the explanatory variables (biochar characteristics). (Biochar and charosphere variables are colored in red and blue, respectively. EC: electrical conductivity; PS: particle size, WP: water extractable phosphorus, Φ: diameter of influence, r: radius of charosphere).

Table 4. Matrix of Pearson correlation coefficients among biochar and charosphere properties

	$pH_{charosphere}$	Φ	r	PS	$pH_{biochar}$	EC	WP	Ash	H/C	O/C
$pH_{charosphere}$	1									
Φ	0.163	1								
r	0.385		1							
PS	-0.163	**0.721****	0.107	1						
$pH_{biochar}$	**0.970****	0.117	0.436	-0.291	1					
EC	**0.611****	**0.580***	**0.717****	0.122	**0.588***	1				
WP	**-0.829****	-0.164	-0.382	0.159	**-0.863****	-0.314	1			
Ash	0.345	-0.416	-0.185	-0.444	0.356	0.123	0.069	1		
H/C	-0.248	-0.224	-0.218	-0.111	-0.230	-0.055	**0.602***	**0.691***	1	
O/C	**-0.934****	0.04	-0.283	0.370	**-0.955****	-0.542	**0.766***	-0.472	0.186	1

Φ: diameter of influence, r: radius of charosphere, PS: particle size, WP: water extractable phosphorus.* and ** indicate significant correlation at $P < 0.05$ (two-tailed) and $P < 0.01$ (two-tailed), respectively. n=12 (3 replicates of each of the 4 biochars studied).

4. Conclusions

Biochar had rapid localized impact on soil pH after soil application, forming charospheres with radius ranging from 1.08 mm to 1.63 mm after 24 h. Within the charosphere, the soil pH gradually changed with distance from biochar over a few hours before reaching equilibrium. Ageing treatment led to significant changes in biochar characteristics, but the change in EC values was the primary factor affecting the charosphere properties. The findings help inform the tailoring of biochar characteristics for different environmental outcomes. Hydroxyapatite engineered biochar has potential to act as a P fertilizer owing to its high P availability. Similarly, ageing treatment may be conducive to P release and enhanced plant nutrition, though the associated decreased biochar pH might increase desorption of PTEs originally adsorbed onto biochar. More in-deep research is needed to investigate the evolution of the charosphere during biochar ageing in relation to the pH thresholds for soil nutrients and predicting the pH-dependent mobility of PTEs.

Declaration of Competing Interest

The authors have no competing interests to declare.

Acknowledgements

X. Chen was funded by the China Scholarship Council and S. Lewis by a UK Natural Environment Research Council (NERC) E3 DTP PhD studentship (grant number NE/L002558/1). The authors would like to thank Dr Ondřej Mašek of the UK Biochar Research Centre (UKBRC) for providing the pH optode, Dr Gavin Sim and John Morman of the School of GeoSciences, University of Edinburgh, for sample analysis, The James Hutton Institute, Scotland, UK, for the

access to the study soil, and the anonymous reviewers for helpful comments that have improved the manuscript.

Appendix A: Supplementary Material

Production of engineered biochar and biochar characteristics (S1). Procedure for planar optode pH calibration (S2). Fourier transform infrared (FTIR) analysis of the study biochars (S3). Redundancy analysis of charosphere properties and biochar characteristics (S4).

Appendix B. Supplementary Data

The video shows the 2D pH values around one of the replicates of the BC_{SE} biochar every 10 minutes as the charosphere develops during the 24 h time period of the experiment. The colors represent different pH values as shown in the legend to Figure 3.

References

Andersson, K.O., Tighe, M.K., Guppy, C.N., Milham, P.J., McLaren, T.I., 2015. Incremental acidification reveals phosphorus release dynamics in alkaline vertic soils. Geoderma 259-260, 35-44. https://doi.org/10.1016/j.geoderma.2015.05.001.

Aller, D., Rathke, S., Laird, D., Cruse, R., Hatfield, J., 2017. Impacts of fresh and aged biochars on plant available water and water use efficiency. Geoderma 307, 114-121. https://doi.org/10.1016/j.geoderma.2017.08.007.

Blossfeld, S., Schreiber, C.M., Liebsch, G., Kuhn, A.J., Hinsinger, P., 2013. Quantitative imaging of rhizosphere pH and CO_2 dynamics with planar optodes. Annals of Botany 112, 267-276.

https://doi.org/10.1093/aob/mct047.

Brabant, I., 2013. An assessment of the effects of biochar ageing on residual function. Undergraduate dissertation. School of GeoSciences, The University of Edinburgh, Edinburgh, UK.

Buss, W., Shepherd, J.G., Heal, K.V., Mašek, O., 2018. Spatial and temporal microscale pH change at the soil-biochar interface. Geoderma 331, 50-52. https://doi.org/10.1016/j.geoderma.2018.06.016.

Chen, X.J., Lin, Q.M., Muhammad, R., Zhao, X.R., Li, G.T., 2019. Steam explosion of crop straws improves the characteristics of biochar as a soil amendment. J. Integr. Agric. 18(7), 1486-1495. https://doi.org/10.1016/S2095-3119(19)62573-6.

Cheng, C.H., Lehmann, J., Engelhard, M.H., 2008. Natural oxidation of black carbon in soils: Changes in molecular form and surface charge along a climosequence. Geochimica et Cosmochimica Acta 72, 1598-1610. https://doi.org/10.1016/j.gca.2008.01.010.

Christel, W., Zhu, K., Hoefer, C., Kreuzeder, A., Santner, J., Bruun, S., Magid, J., Jensen, L.S., 2016. Spatiotemporal dynamics of phosphorus release, oxygen consumption and greenhouse gas emissions after localised soil amendment with organic fertilisers. Sci. Total Environ. 554-555, 119-129. https://doi.org/10.1016/j.scitotenv.2016.02.152.

Cross, A., Sohi, S.P., 2013. A method for screening the relative long-term stability of biochar. GCB Bioenergy 5, 215-220. https://doi.org/10.1111/gcbb.12035.

de la Rosa, J.M., Rosado, M., Paneque, M., Miller, A.Z., Knicker, H., 2018. Effects of aging under field conditions on biochar structure and composition: Implications for biochar stability in soils. Sci. Total Environ. 613-614, 969-976. https://doi.org/10.1016/j.scitotenv.2017.09.124.

Duan, W.Y., Oleszczuk, P., Pan, B., Xing, B.S., 2019. Environmental behavior of engineered biochars and their aging processes in soil. Biochar 1, 339-351. https://doi.org/10.1007/s42773-019-

521 00030-5.

522 Faget, M., Blossfeld, S., von Gillhaussen, P., Schurr, U., Temperton, V.M., 2013. Disentangling who
523 is who during rhizosphere acidification in root interactions: combining fluorescence with optode
524 techniques. Frontiers in Plant Sci. 4, 1-8. https://doi.org/10.3389/fpls.2013.00392.

525 FAOstat, 2018. Food and Agriculture Organization of the United Nations,
526 http://www.fao.org/faostat/en/#data/QC (accessed 9 December 2020).

527 Feng, M.Y., Zhang, W.H., Wu, X.Y., Jia, Y.M., Jiang, C.X., Wei, H., Qiu, R.L., Tsang, D.C.W., 2018.
528 Continuous leaching modifies the surface properties and metal(loid) sorption of sludge-derived
529 biochar. Sci. Total Environ. 625, 731-737. https://doi.org/10.1016/j.scitotenv.2017.12.337.

530 Gámiz, B., Velarde, P., Spokas, K.A., Celis, R., Cox, L., 2019. Changes in sorption and
531 bioavailability of herbicides in soil amended with fresh and aged biochar. Geoderma 337, 341-349.
532 https://doi.org/10.1016/j.geoderma.2018.09.033.

533 He, Y., Liu, C., Tang, X.Y., Xian, Q.S., Zhang, J.Q., Guan, Z., 2019. Biochar impacts on sorption-
534 desorption of oxytetracycline and florfenicol in an alkaline farmland soil as affected by field ageing.
535 Sci. Total Environ. 671, 928-936. https://doi.org/10.1016/j.scitotenv.2019.03.414.

536 Houben, D., Sonnet, P., 2015. Impact of biochar and root-induced changes on metal dynamics in the
537 rhizosphere of *Agrostis capillaris* and *Lupinus albus*. Chemosphere 139, 644-651.
538 https://doi.org/10.1016/j.chemosphere.2014.12.036.

539 Huff, M.D., Lee, J.W., 2016. Biochar-surface oxygenation with hydrogen peroxide. J. Environ.
540 Manag. 165, 17-21. https://doi.org/10.1016/j.jenvman.2015.08.046.

541 Jing, F.Q., Sohi, S.P., Liu, Y.Y., Chen, J.W., 2018. Insight into mechanism of aged biochar for
542 adsorption of PAEs: Reciprocal effects of ageing and coexisting Cd^{2+}. Environ. Pollut. 242, 1098-

543 1107. https://doi.org/10.1016/j.envpol.2018.07.124.

544 Kambo, H.S., Dutta, A., 2015. A comparative review of biochar and hydrochar in terms of
545 production, physico-chemical properties and applications. Renew. Sust. Energ. Rev. 45, 359-378.
546 https://doi.org/10.1016/j.rser.2015.01.050.

547 Kätterer, T., Roobroeck, D., Andrén, O., Kimutai, G., Karltun, E., Kirchmann, H., Nyberg, G.,
548 Vanlauwe, B., de Nowina, K., 2019. Biochar addition persistently increased soil fertility and yields
549 in maize-soybean rotations over 10 years in sub-humid regions of Kenya. Field Crops Res. 235, 18-
550 26. https://doi.org/10.1016/j.fcr.2019.02.015.

551 Koop-Jakobsen, K., Mueller, P., Meier, R.J., Liebsch, G., Jensen, K., 2018. Plant-sediment
552 interactions in salt marshes - an optode imaging study of O_2, pH, and CO_2 gradients in the
553 rhizosphere. Frontiers in Plant Sci. 9, 1-11. https://doi.org/10.3389/fpls.2018.00541.

554 Kumar, A., Joseph, S., Tsechansky, L., Privat, K., Schreiter, I., Schüth, C., Graber, E., 2018. Biochar
555 aging in contaminated soil promotes Zn immobilization due to changes in biochar surface structural
556 and chemical properties. Sci. Total Environ. 626, 953-961.
557 https://doi.org/10.1016/j.scitotenv.2018.01.157.

558 Kuzyakov, Y., Blagodatskaya, E., 2015. Microbial hotspots and hot moments in soil: concept &
559 review. Soil Biol. Biochem. 83, 184-199. https://doi.org/10.1016/j.soilbio.2015.01.025.

560 Kuzyakov, Y., Razavi, B.S., 2019. Rhizosphere size and shape: temporal dynamics and spatial
561 stationarity. Soil Biol. Biochem. 135, 343-360. https://doi.org/10.1016/j.soilbio.2019.05.011.

562 Lehmann, J., Rillig, M.C., Thies, J., Masiello, C.A., Hockaday, W.C., Crowley, D., 2011. Biochar
563 effects on soil biota - a review. Soil Biol. Biochem. 43, 1812-1836. https://doi.org/
564 10.1016/j.soilbio.2011.04.022.

565 Li, C., Ding, S.M., Yang, L.Y., Zhu, Q.Z., Chen, M.S., Tsang, D.C.W., Cai, G., Feng, C., Wang, Y.,
566 Zhang, C.S., 2019. Planar optode: A two-dimensional imaging technique for studying spatial-
567 temporal dynamics of solutes in sediment and soil. Earth-Sci. Rev. 197, 102916.
568 https://doi.org/10.1016/j.earscirev.2019.102916.
569 Li, H.X., Lu, X.Q., Xu, Y., Liu, H.T., 2019. How close is artificial biochar aging to natural biochar
570 aging in fields? A meta-analysis. Geoderma 352, 96-103.
571 https://doi.org/10.1016/j.geoderma.2019.06.006.
572 Liu, Y.Y., Sohi, S.P., Jing, F.Q., Chen, J.W., 2019. Oxidative ageing induces change in the
573 functionality of biochar and hydrochar: Mechanistic insights from sorption of atrazine. Environ.
574 Pollut. 249, 1002-1010. https://doi.org/10.1016/j.envpol.2019.03.035.
575 Luo, Y., Durenkamp, M., Nobili, M.D., Lin, Q.M., Devonshire, B.J., Brookes, P.C., 2013. Microbial
576 biomass growth, following incorporation of biochars produced at 350 °C or 700 °C, in a silty-clay
577 loam soil of high and low pH. Soil Biol. Biochem. 57, 513-523.
578 https://doi.org/10.1016/j.soilbio.2012.10.033.
579 Melo, L.C.A., Puga, A.P., Coscione, A.R., Beesley, L., Abreu, C.A., Camargo, O.A., 2016. Sorption
580 and desorption of cadmium and zinc in two tropical soils amended with sugarcane-straw-derived
581 biochar. J. Soils & Sediments 16, 226-234. https://doi.org/10.1007/s11368-015-1199-y.
582 Naisse, C., Alexis, M., Plante, A., Wiedner, K., Glaser, B., Pozzi, A., Carcaillet, C., Criscuoli, I.,
583 Rumpel, C., 2013. Can biochar and hydrochar stability be assessed with chemical methods? Org.
584 Geochem. 60, 40-44. https://doi.org/10.1016/j.orggeochem.2013.04.011.
585 Neina, D., 2019. The role of soil pH in plant nutrition and soil remediation. Appl. & Environ. Soil
586 Sci. https://doi.org/10.1155/2019/5794869.

Pastore, G., Kaiser, K., Kernchen, S., Spohn, M., 2020. Microbial release of apatite- and goethite-bound phosphate in acidic forest soils. Geoderma 370, 114360. https://doi.org/10.1016/j.geoderma.2020.114360.

Pereira, R.C., Arbestain, M.C., Sueiro, M.V., Maciá-Agulló, J.A., 2015. Assessment of the surface chemistry of wood-derived biochars using wet chemistry, Fourier transform infrared spectroscopy and X-ray photoelectron spectroscopy. Soil Res. 53, 753-762. https://doi.org/10.1071/SR14194.

Prendergast-Miller, M.T., Duvall, M., Sohi, S.P., 2014. Biochar-root interactions are mediated by biochar nutrient content and impacts on soil nutrient availability. Eur. J. Soil Sci. 65, 173-185. https://doi.org/10.1111/ejss.12079.

Quilliam, R.S., Glanville, H.C., Wade, S.C., Jones, D.L., 2013. Life in the 'charosphere'-Does biochar in agricultural soil provide a significant habitat for microorganisms? Soil Biol. Biochem. 65, 287-293. https://doi.org/10.1016/j.soilbio.2013.06.004.

Rechberger, M.V., Kloss, S., Rennhofer, H., Tintner, J., Watzinger, A., Soja, G., Lichtenegger, H., Zehetner, F., 2017. Changes in biochar physical and chemical properties: Accelerated biochar aging in an acidic soil. Carbon 115, 209-219. https://doi.org/10.1016/j.carbon.2016.12.096.

Rechberger, M.V., Kloss, S., Wang, S.L., Lehmann, J., Rennhofer, H., Ottner, F., Wriessnig, K., Daudin, G., Lichtenegger, H., Soja, G., Zehetner, F., 2019. Enhanced Cu and Cd sorption after soil aging of woodchip-derived biochar: What were the driving factors? Chemosphere 216, 463-471. https://doi.org/10.1016/j.chemosphere.2018.10.094.

Santner, J., Larsen, M., Kreuzeder, A., Glud, R.N., 2015. Two decades of chemical imaging of solutes in sediments and soils - a review. Analytica Chimica Acta 878, 9-42. https://doi.org/10.1016/j.aca.2015.02.006.

609 Sauzet, O., Cammas, C., Gilliot, J.M., Bajard, M., Montagne, D., 2017. Development of a novel
610 image analysis procedure to quantify biological porosity and illuvial clay in large soil thin sections.
611 Geoderma 292, 135-148. https:/doi.org/10.1016/j.geoderma.2017.01.004.
612 Schimmelpfennig, S., Glaser, B., 2012. One step forward toward characterization: some important
613 material properties to distinguish biochars. J. Environ. Qual. 41, 1001-1013.
614 https://doi.org/10.2134/jeq2011.0146.
615 Spokas, K.A., Novak, J.M., Masiello, C.A., Johnson, M.G., Colosky, E.C., Ippolito, J.A., Trigo, C.,
616 2014. Physical disintegration of biochar: an overlooked process. Environ. Sci. Technol. Lett. 1, 326-
617 332. https:// doi.org/10.1021/ez500199t.
618 Spokas, K.A., Novak, J.M., Masiello, C.A., Johnson, M.G., Colosky, E.C., Ippolito, J.A., Trigo, C.,
619 2014. Physical disintegration of biochar: an overlooked process. Environ. Sci. Technol. Lett. 1, 326-
620 332. https:// doi.org/10.1021/ez500199t.
621 Sun, X., Li, Z., Wu, L.H., Christie, P., Luo, Y.M., Fornara, D.A., 2019. Root-induced soil
622 acidification and cadmium mobilization in the rhizosphere of *Sedum plumbizincicola*: evidence
623 from a high-resolution imaging study. Plant & Soil 436, 267-282. https://doi.org/10.1007/s11104-
624 018-03930-w.
625 Sun, Z.C., Zhang, Z.C., Zhu, K., Wang, Z.M., Zhao, X.R., Lin, Q.M., Li, G.T., 2020. Biochar altered
626 native soil organic carbon by changing soil aggregate size distribution and native SOC in aggregates
627 based on an 8-year field experiment. Sci. Total Environ. 708, 134829.
628 https://doi.org/10.1016/j.scitotenv.2019.134829.
629 Tan, L.S., Ma, Z.H., Yang, K.Q., Cui, Q.L., Wang, K., Wang, T.T., Wu, G.L., Zheng, J.Y., 2020.
630 Effect of three artificial aging techniques on physicochemical properties and Pb adsorption

631 capacities of different biochars. Sci. Total Environ. 699, 134223.
632 https://doi.org/10.1016/j.scitotenv.2019.134223.
633 Wang, L., Meng, J., Li, Z.T., Liu, X.M., Xia, F., Xu, J.M., 2017. First "charosphere" view towards
634 the transport and transformation of Cd with addition of manure derived biochar. Environ. Pollut.
635 227, 175-182. https://doi.org/10.1016/j.envpol.2017.04.024.
636 Williams, P.N., Santner, J., Larsen, M., Lehto, N.J., Oburger, E., Wenzel, W., Glud, R.N., Davison,
637 W., Zhang, H., 2014. Localized flux maxima of arsenic, lead, and iron around root apices in flooded
638 lowland rice. Environ. Sci. Technol. 48, 8498-8506. https://doi.org/10.1021/es501127k.
639 Wu, S.W., Zhang, Y., Tan, Q., Sun, X.C., Wei, W.H., Hu, C.X., 2020. Biochar is superior to lime in
640 improving acidic soil properties and fruit quality of Satsuma mandarin. Sci. Total Environ. 714,
641 136722. https://doi.org/10.1016/j.scitotenv.2020.136722.
642 Yang, Z.M., Fang, Z.Q., Zheng, L.C., Cheng, W., Tsang, P.E., Fang, J.Z., Zhao, D.Y., 2016.
643 Remediation of lead contaminated soil by biochar-supported nano-hydroxyapatite. Ecotoxicol. &
644 Environ. Saf. 132, 224-230. https://doi.org/10.1016/j.ecoenv.2016.06.008.
645 Yi, Q.Q., Liang, B.Q., Nan, Q., Wang, H., Zhang, W., Wu, W.X., 2020. Temporal physicochemical
646 changes and transformation of biochar in a rice paddy: Insights from a 9-year field experiment. Sci.
647 Total Environ. 721, 137670. https://doi.org/10.1016/j.scitotenv.2020.137670.
648 Yu, M.J., Meng, J., Yu, L., Su, W.Q., Afzal, M., Li, Y., Brookes, P.C., Redmile-Gordon, M., Luo, Y.,
649 Xu, J.M., 2019. Changes in nitrogen related functional genes along soil pH, C and nutrient gradients
650 in the charosphere. Sci. Total Environ. 650, 626-632.
651 https://doi.org/10.1016/j.scitotenv.2018.08.372.